Analysis and Implementation of an Improved Current-Doubler Rectifier With Coupled Inductors

Tsai-Fu Wu, *Senior Member, IEEE*, Cheng-Tao Tsai, Yong-Dong Chang, and Yaow-Ming Chen, *Senior Member, IEEE*

***Abstract*—In this paper, an improved current-doubler rectifier with coupled inductors is proposed. The proposed rectifier can extend duty ratio to reduce the peak current through the isolation transformer winding and lower output current ripple as well as voltage stress of the rectifier diodes. In this study, a 500-W prototype with a full-bridge phase-shift converter, the proposed rectifier, with input voltage of 400 V and output voltage of 12 V was built. Theoretical analysis and experimental results have verified that the proposed rectifier is attractive for high step-down voltage and high-power applications.**

***Index Terms*—Coupled inductors, current-doubler rectifier, full-bridge phase-shift converter, isolation transformer, tapped inductor.**

I. Introduction

In order to meet the requirement of high speed and low loss, operating voltage of a high-performance microprocessor is gradually decreased from 5 to 3.3 V. It will even drop below 1 V, and the current will go beyond 100 A in the future. Therefore, point-of-load dc–dc converters will use 5 or 12 V as the major input voltage to reduce distribution loss [1], and an isolated dc–dc converter with high step-down voltage ratio, high output current, and high efficiency is usually required, as shown in the shaded area of Fig. 1.

To achieve low output voltage, high output current, and high efficiency, the active clamp interleaved forward converter [2]–[4] has been widely adopted, since it can realize zero-voltage switching (ZVS), reduce electromagnetic interference (EMI), and lower output current ripple. However, the transformers are not fully utilized, and the filter inductors at their secondary sides suffer from high current stresses and thermal problems, which result in low step-down voltage ratio and low power density. The conventional full-bridge phase-shift current-doubler converter [5] can provide a straightforward solution for the problems, because of its simple structure, constant frequency pulsewidth modulation (PWM) control, high current capability, and low switching loss. Nevertheless, it still has several limitations, such as for high step-down voltage conversion, it requires a transformer with high turns ratio or it has to reduce the duty ratio of the switches. A high turns ratio will result in high duty loss and low conversion efficiency, while a low duty ratio will increase input peak current and component stress [6]. The other limitation is that its large external resonant inductor will induce a large circulation current, which will flow through the primary winding of the transformer and switches during a freewheeling interval. As a result, conduction loss in the switches and copper loss in the transformer are significant. Moreover, another major limitation is the resonance of diode junction capacitance with transformer leakage inductance, which results in voltage oscillation and reverse recovery loss. To overcome the aforementioned limitations of the conventional full-bridge current-doubler converter, many approaches [7]–[11] have been conducted. However, their high step-down voltage ratios still result in extreme low duty ratios that will induce high peak current through the secondary winding of the isolation transformer and output filter inductors, increasing copper loss and component stress.

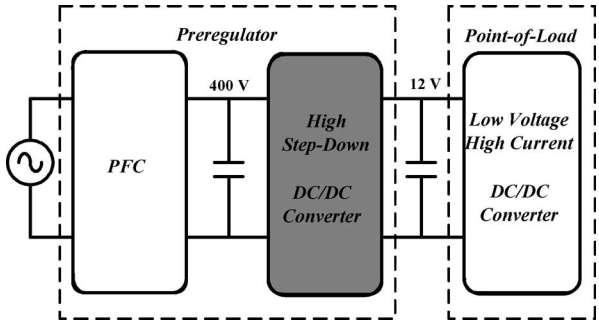

Fig. 1. Distributed power system structure.

In this paper, an improved current-doubler rectifier with coupled inductors is proposed, as shown in Fig. 2. In comparison with the conventional current-doubler rectifier (CCDR) [5], the component counts of the proposed rectifier are identical, while the proposed rectifier can adjust the turns ratio of the coupled inductor to extend the duty ratio range, which can reduce the peak current through the isolation transformer and switches, and can lower output current ripple. Additionally, the rectifier diodes can be operated with low voltage stress, which, in turn, can reduce reverse recovery loss. The operating frequency can then be increased significantly.

Section II describes derivation and operational principle of the proposed current-doubler rectifier. Section III demonstrates the benefits of the proposed rectifier and its comparison with the CCDR. Design considerations and power loss estimations are presented in Sections IV and V. Simulation and experimental

Manuscript received June 13, 2007; revised August 27, 2007. First published October 28, 2008; current version published December 9, 2008. Recommended for publication by Associate Editor F. L. Luo.

T.-F. Wu, C.-T. Tsai, and Y.-M. Chen are with the Elegant Power Application Research Center (EPARC), Department of Electrical Engineering, National Chung Cheng University, Chia-Yi 621, Taiwan (e-mail: tfwu@ee.ccu.edu.tw).

Y.-D. Chang is with the Department of Electrical Engineering, Kun Shan University, Tainan 710, Taiwan, and also with the Elegant Power Application Research Center (EPARC), Department of Electrical Engineering, National Chung Cheng University, Chia-Yi 621, Taiwan.

Digital Object Identifier 10.1109/TPEL.2008.2005372

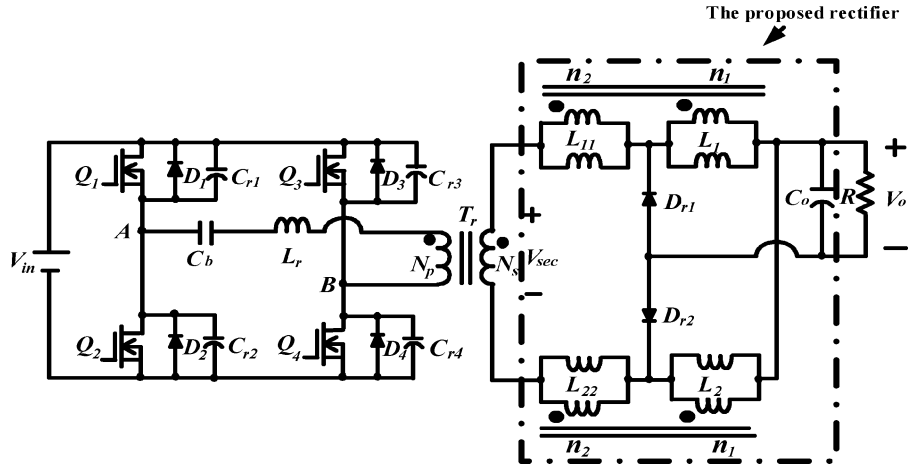

Fig. 2. Proposed current-doubler rectifier with a full-bridge phase-shift converter.

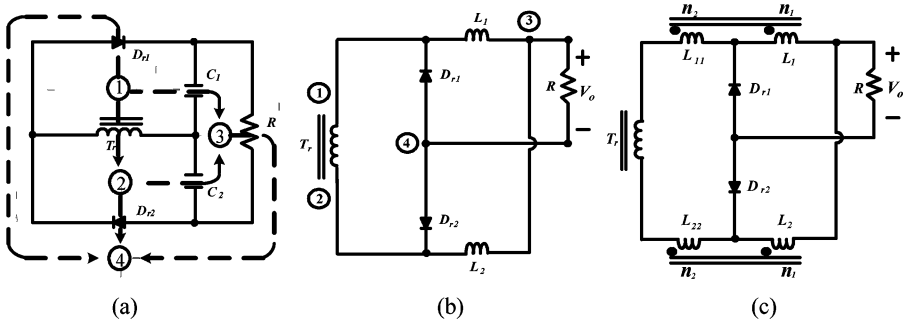

Fig. 3. Derivation of the proposed current doubler from a voltage doubler based on duality. (a) Voltage doubler. (b) Derived current doubler without coupling inductors. (c) Proposed current doubler with coupled inductors.

results obtained from a 500-W prototype with the proposed current-doubler rectifier and the full-bridge phase-shift converter are presented in Section VI to verify its feasibility. Finally, a conclusion is given in Section VII.

II. Derivation and Operational Principle

Derivation of the proposed current-doubler rectifier is based on a conventional voltage-doubler circuit, as illustrated in Fig. 3(a). According to duality, meshes of the voltage doubler are replaced with nodes, and capacitors are replaced with inductors, while diodes are with no change, yielding the current-doubler rectifier, as depicted in Fig. 3(b). In Fig. 3(b), the output filter inductors can be extended to the coupled ones, as shown in Fig. 3(c). Each coupled inductor individually functions as a tapped inductor or a transformer during one switching cycle. In other words, the upper coupled inductor is charged during the charging period, which functions as a tapped inductor, while the lower coupled inductor functions as a transformer. Therefore, the proposed rectifier with coupled inductors can widen duty ratio range, lower output current ripple, and lower voltage stress of the rectifier diode over that of the CCDR.

The proposed current-doubler rectifier based on a full-bridge phase-shift converter is illustrated in Fig. 2. It mainly includes two sets of coupled inductors L_1 and L_2, free-wheeling diodes D_{r1} and D_{r2}, and an output filter capacitor C_o. Each set of the coupled inductors can be treated as a transformer with two magnetizing inductors, and its turns ratio is defined as

$$n = \frac{(n_1 + n_2)}{n_1}, \qquad n \geq 1. \tag{1}$$

To simplify description of the steady-state operational modes, the full-bridge phase-shift converter will not be discussed in this section. Only the proposed current-doubler rectifier is analyzed, and we have the following assumptions.

1) All of the switching devices and diodes are ideal.
2) Inductance $L_1 = L_2$ and $L_{11} = L_{22}$.
3) Leakage inductance of the coupled inductors is much smaller than the resonant inductor L_r and can be neglected from the successive analysis.
4) The output filter capacitor C_o is large enough so that it can be treated as a voltage source V_o.

Under continuous inductor current operation, six major operating modes are identified over one switching cycle. Fig. 4 shows conceptual voltage and current waveforms of its key components. $D_{\rm eff}$ and $D_{\rm loss}$ are denoted as the effective and lost duty ratios, respectively, V_{AB} is the voltage across the resonant inductor and the isolation transformer primary winding, $V_{\rm sec}$ is the voltage across the isolation transformer secondary winding, $i_{\rm sec}$ is the secondary current, i_L and V_L are the current and voltage of the coupled inductor winding n_1, i_{Dr} and V_{Dr} are the current and voltage of the rectifier diode, and i_o is the

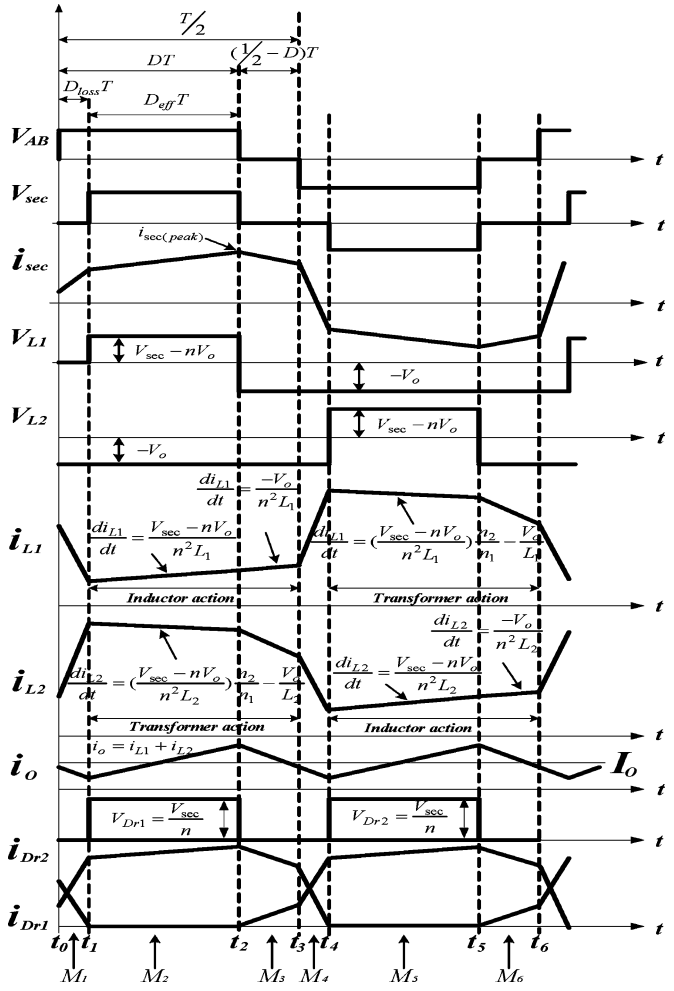

Fig. 4. Key waveforms of the proposed converter shown in Fig. 2.

output current. Fig. 5 shows equivalent circuits of the operational modes.

Mode 1 [Fig. 5(a), $t_o \le t < t_1$]: At time t_0, currents i_{Dr1} and i_{Dr2} are commutated completely. Then, a positive voltage $V_{\rm sec}$ crosses the secondary winding of transformer T_r, diode D_{r1} is reversely biased, and inductor current i_{L1} flowing through the path $V_o - D_{r2} - L_{22} - V_{\rm sec} - L_{11} - L_1$ is linearly increased. During this interval, the energy stored in inductor L_{22} will be released to the load through coupled inductor L_2, and inductor current i_{L2} flowing through the path $V_o - D_{r2}$ is decreased. Meanwhile, inductors L_{11} and L_1 function as a tapped inductor, while inductors L_{22} and L_2 are coupled to function as a transformer. The coupled inductor currents and the rectifier diode voltages can be expressed as follows:

$$i_{L1}(t) = \frac{V_{\rm sec} - nV_o}{n^2 L_1}(t - t_0) + i_{L1}(t_0) \tag{2}$$

$$i_{L2}(t) = i_{L2}(t_0) + \left(\frac{V_{\rm sec} - nV_o}{n^2 L_1}\right)\left(\frac{n_2}{n_1}\right)(t - t_0) - \frac{V_o}{L_2}(t - t_0) \tag{3}$$

$$V_{Dr1} = \frac{V_{\rm sec}}{n} \tag{4}$$

and

$$V_{Dr2} = 0. \tag{5}$$

Mode 2 [Fig. 5(b), $t_1 \le t < t_2$]: When voltage $V_{\rm sec}$ drops to zero at time t_1, the energy stored in inductor L_{22} is no longer released to the load through coupled inductor L_2. Therefore, inductor current i_{L2} will be gradually decreased, rectifier diodes D_{r1} and D_{r2} are conducted, and rectifier diode currents i_{Dr1} and i_{Dr2} begin commutating. During this freewheeling interval, inductor currents i_{L1} and i_{L2} are decreased linearly. The coupled-inductor currents and the rectifier diode voltages can be expressed as follows:

$$i_{L1}(t) = i_{L1}(t_1) - \frac{V_o}{n^2 L_1}(t - t_1) \tag{6}$$

$$i_{L2}(t) = i_{L2}(t_1) - \frac{V_o}{L_2}(t - t_1) \tag{7}$$

and

$$V_{Dr1} = V_{Dr2} = 0. \tag{8}$$

Mode 3 [Fig. 5(c), $t_2 \le t < t_3$]: At time t_2, a negative voltage V_{AB} will cross the resonant inductor L_r and the primary winding of transformer T_r, since rectifier diode currents i_{Dr1} and i_{Dr2} have not yet been commutated completely. Therefore, the two rectifier diodes D_{r1} and D_{r2} are maintained in conducting state, while inductors L_1 and L_2 are discharged through diodes D_{r1} and D_{r2}, respectively.

Mode 4 [Fig. 5(d), $t_3 \le t < t_4$]: At time t_3, currents i_{Dr1} and i_{Dr2} are commutated completely, diode D_{r2} is reversely biased, and inductor current i_{L2} flowing through the path $V_o - D_{r1} - L_{11} - V_{\rm sec} - L_{22} - L_2$ is linearly increased. During this interval, the energy stored in inductor L_{11} is released to the load through coupled inductor L_1, and inductor current i_{L1} flowing through the path $V_o - D_{r1}$ is decreased. Over this time interval, inductors L_{22} and L_2 function as a tapped inductor, while inductors L_{11} and L_1 are coupled to function as a transformer. The coupled-inductor currents and the rectifier diode voltages can be expressed as follows:

$$i_{L1}(t) = i_{L1}(t_3) + \left(\frac{V_{\rm sec} - nV_o}{n^2 L_2}\right)\left(\frac{n_2}{n_1}\right)(t - t_3) - \frac{V_o}{L_1}(t - t_3) \tag{9}$$

$$i_{L2}(t) = \left(\frac{V_{\rm sec} - nV_o}{n^2 L_2}\right)(t - t_3) + i_{L1}(t_3) \tag{10}$$

$$V_{Dr1} = 0 \tag{11}$$

and

$$V_{Dr2} = \frac{V_{\rm sec}}{n}. \tag{12}$$

Mode 5 [Fig. 5(e), $t_4 \le t < t_5$]: At time t_4, voltage $V_{\rm sec}$ drops to zero, rectifier diodes D_{r1} and D_{r2} are conducting, and rectifier diode currents i_{Dr1} and i_{Dr2} begin commutating. During this freewheeling interval, inductor currents i_{L1} and i_{L2} are decreased linearly. The coupled-inductor currents and the

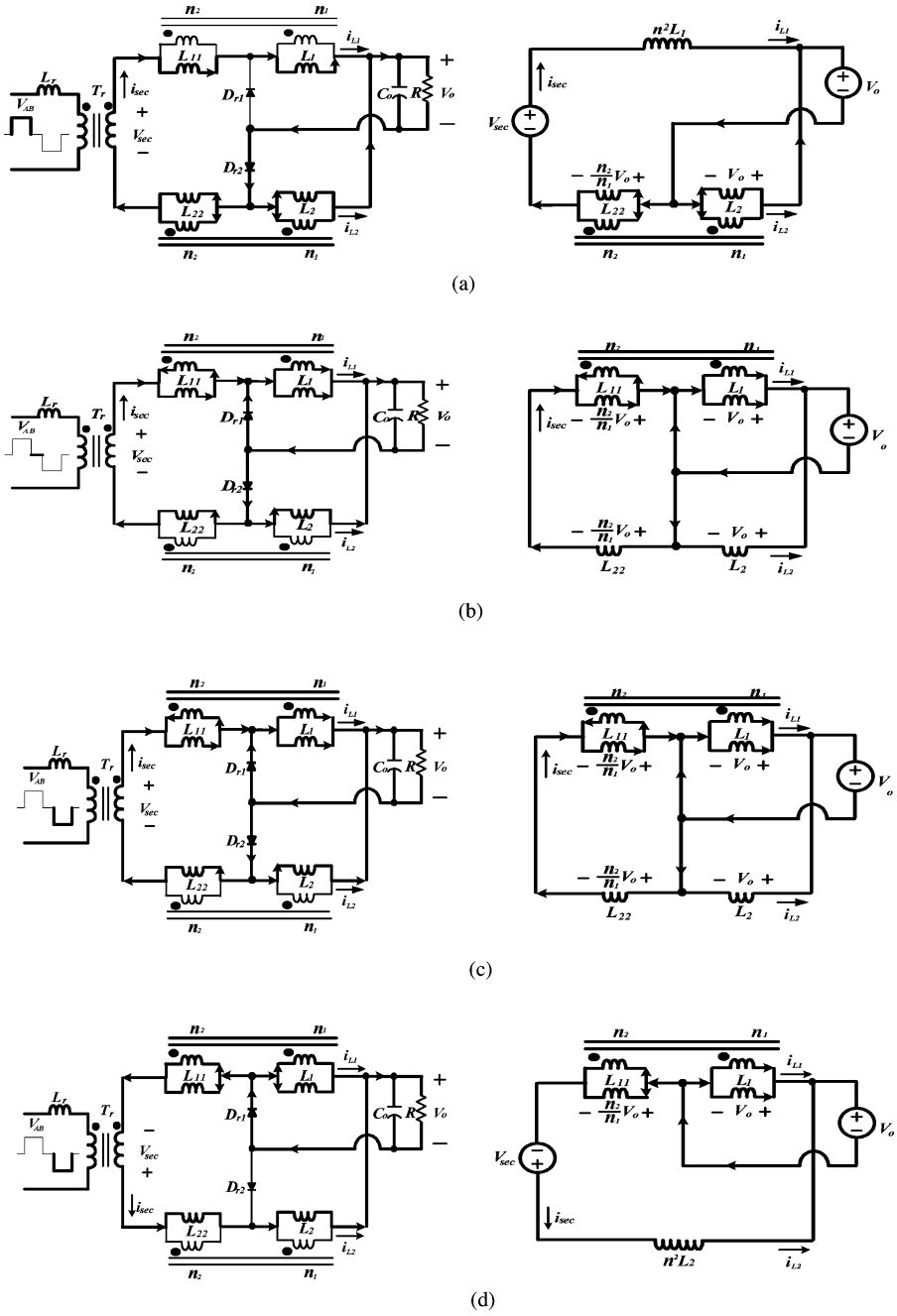

Fig. 5. Equivalent circuits of the operation modes.

rectifier diode voltages can be expressed as follows:

$$i_{L1}(t) = i_{L1}(t_4) - \frac{V_o}{L_1}(t - t_4) \tag{13}$$

$$i_{L2}(t) = i_{L2}(t_4) - \frac{V_o}{n^2 L_2}(t - t_4) \tag{14}$$

and

$$V_{Dr1} = V_{Dr2} = 0. \tag{15}$$

Mode 6 [Fig. 5(f), $t_5 \le t < t_6$]: At time t_5, a positive voltage V_{AB} crosses the resonant inductor L_r and primary winding of transformer T_r again, since rectifier diode currents i_{Dr1} and i_{Dr2} have not yet been commutated completely. Therefore, rectifier diodes D_{r1} and D_{r2} are maintained conducting, while inductors L_1 and L_2 are discharged through diodes D_{r1} and D_{r2}, respectively. The operational principle over one switching cycle is completed.

III. Features and Characteristics

This section describes the features and characteristics of the proposed rectifier, which include voltage gain, diode voltage stress, and output current ripple. To highlight the merits of the proposed rectifier, its performance indexes are discussed and compared with those of the CCDR [5].

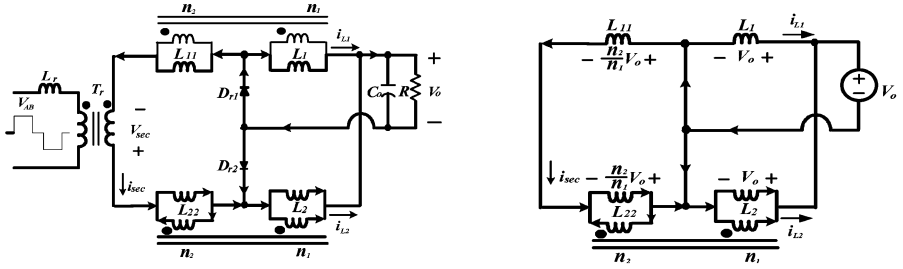

(e)

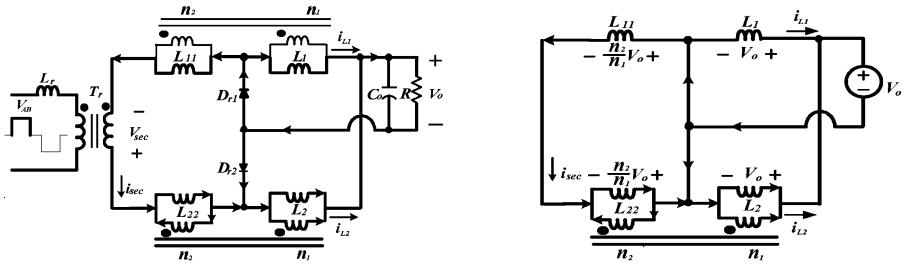

(f)

Fig. 5. (*Continued*).

A. Voltage Gain

In Fig. 4, from the current equations of inductors L_1 and L_2 and by applying the volt·seconds balance principle, the voltage gain and diode voltage stress can be derived as

$$\frac{V_o}{V_{\rm sec}} = \frac{2D}{n(1+n)} \tag{16}$$

where D is the duty ratio of the active switches and $D < 0.5$. There is one assumption that the lost duty ratio is smaller than the effective duty ratio (i.e., $D_{\rm loss} << D_{\rm eff}$); hence, $D \approx D_{\rm eff}$.

B. Voltage Stress of the Rectifier Diode

At mode 1, rectifier diode D_{r1} stays in the OFF state, while D_{r2} is conducting. At mode 4, the states of D_{r1} and D_{r2} are exchanged. Their voltage stress can be derived as

$$V_{Dr1} = V_{Dr2} = \frac{V_{\rm sec}}{n}. \tag{17}$$

C. Output Current Ripple

From Fig. 4 and by combining the currents of i_{L1} and i_{L2}, output current ripple can be determined as

$$i_{\rm ripple} = \left[\frac{(1+n)}{2} - 2D\right]\frac{V_o}{Lf_s} \tag{18}$$

where f_s is the switching frequency of the active switches and inductance $L = L_1 = L_2$.

In (16)–(18), turns ratio $n = 1$ corresponds to a CCDR.

From (16), we can sketch a set of curves showing the relationship between duty ratio D and the voltage ratio of $V_o/V_{\rm sec}$ for different values of turns ratio n, as illustrated in Fig. 6. Fig 7 shows the plot of diode voltage stress versus n according to (17). Fig. 8 shows the plot of output current ripple $i_{\rm ripple}$ (%) versus n according to (18), from which it can be seen that the turns ratio

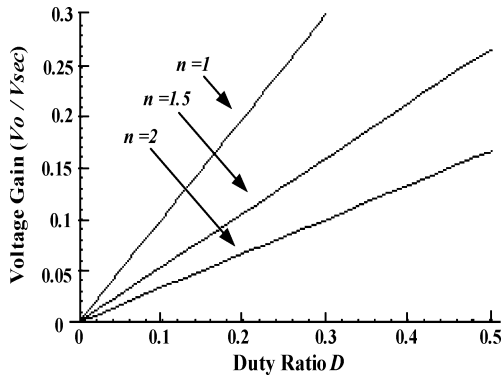

Fig. 6. Plots $V_o/V_{\rm sec}$ versus duty ratio D.

of coupled inductor $n = 2$ is not a good choice, because it yields higher output current ripple. To objectively judge the merits of the proposed current-doubler rectifier, performance comparison between the proposed rectifier and the CCDR is shown in Table I, and an example with $n = 1.5$ and identical voltage gain ($V_o/V_{\rm sec}$) is shown in Fig. 9. From these plots, it can be seen that the proposed current-doubler rectifier under full-load condition yields higher duty ratio, lower current ripple, and lower diode voltage stress over the conventional one.

IV. Design Considerations

To verify the performance of the proposed current-doubler rectifier, a 500-W prototype with a full-bridge phase-shift converter and the proposed rectifier was designed and built. Its specifications are listed as follows:

1) input voltage $V_{\rm in}$: 360–400 $V_{\rm dc}$;
2) output voltage V_o: 12 $V_{\rm dc}$;
3) maximum output current I_o: 42 A;
4) output voltage ripple ΔV_o: 0.12 V;
5) switching frequency f_s: 100 kHz.

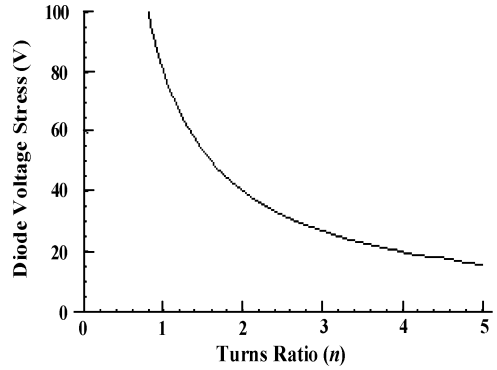

Fig. 7. Plots of diode voltage stress versus turns ratio n of the coupled inductor.

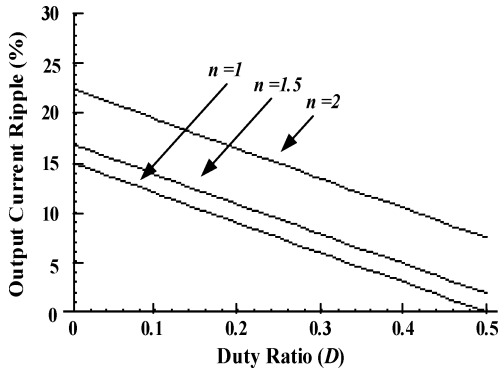

Fig. 8. Plots of output current ripple (%) versus turns ratio n of the coupled inductor.

TABLE I
COMPARISON BETWEEN THE PROPOSED RECTIFIER AND THE CCDR

	Conventional Current Doubler	Proposed Current Doubler
Voltage Gain	$\frac{V_o}{V_{sec}} = D_m$	$\frac{V_o}{V_{sec}} = \frac{2D_n}{n(1+n)}$
Diode Voltage Stress	$V_{Dr} = V_{sec}$	$V_{Dr} = \frac{V_{sec}}{n}$
Output Current Ripple	$i_{o(ripple)} = (1-2D_m)\frac{V_o}{Lf_s}$	$i_{o(ripple)} = (\frac{1+n}{2}-2D_n)\frac{V_o}{Lf_s}$

Note: D_m and D_n are the maximum duty ratio of the conventional current doubler and the proposed current doubler, respectively.

In Fig. 2, the key parameters and components can be determined from the design procedure shown as follows.

A. Design of the Coupled Inductors

A higher turns ratio results in higher leakage inductance that causes a severe voltage spike across the rectifier diodes and increases power loss. Additionally, according to (3) or (9), we can plot the output current ripple waveforms of the coupled inductors, as shown in Fig. 10. When $n_2 > n_1$, current ripples (Δi_{L1} and Δi_{L2}) of the coupled inductors will increase. Since a larger current ripple will result in larger core loss in the coupled inductors, a high turns ratio is not desirable. In this study, we choose $n = 1.5$.

In the design, the turns ratio of the isolation transformer is chosen as $N_p : N_s = 5 : 1$; thus, the secondary voltage $V_{\rm sec}$ will vary from 72 to 80 V. From (16) to (18), we can obtain effective maximum duty ratio $D_{\max} = 0.31$ and minimum duty ratio $D_{\min} = 0.28$, maximum diode voltage stress $V_{Dr} = 53.3$ V, and output current ripple $i_{\rm ripple} = (9\%)I_o = 3.78$ A. Based on (18), the inductance $L = L_1 = L_2$ can be determined as

$$L = \left(\frac{1+n}{2} - 2D_{\max}\right)\frac{V_o}{i_{\rm ripple} f_s} = 16.7\ \mu\text{H}. \tag{19}$$

The inductance $L = 20\ \mu$H is selected. When the turns ratio $n = (n_1 + n_2)/n_1$ is equal to 1.5, inductance $L_{11} = L_{22}$ can be determined as

$$L_{11} = L_{22} = \frac{n_2^2}{n_1^2}L = (n-1)^2 L = 5\ \mu\text{H}. \tag{20}$$

B. Design of the Isolation Transformer

In the design, we first choose ferrite material of TDK PC40 and maximum flux $B_{\max} = 200$ mT, maximum winding factor $K_{w(\max)} = 0.3$, and maximum current density $J_{\max} = 400\,\text{A/cm}^2$. Therefore, the area product of the core can be determined as

$$A_p = W_a A_e > \frac{[P_o + (P_o/\eta)] \times 10^4}{2B_{\max} K_{w(\max)} J_{\max} f_s} = 2.08\ \text{cm}^4 \tag{21}$$

where W_a is the window area of the core, A_e is the effective cross-section area of the core, P_o is the output power of the converter, and η denotes the efficiency. From the TDK data book, we select a proper size of core ETD-44 ($A_e = 1.75\,\text{cm}^2$, $W_a = 3.05\,\text{cm}^2$, $V_e = 18\,\text{cm}^3$, and $A_L = 4000\ \text{nH/N}^2$) to minimize the core loss.

By applying Faraday's law, the turns of the primary winding of the isolation transformer can be determined as

$$N_p \geq \frac{V_{\text{in(min)}} D_{\max}}{2B_{\max} A_e f_s} = 15.4. \tag{22}$$

In this design, N_p is chosen as 20. Therefore, the turns of the secondary winding can be correspondingly determined as

$$N_s = N_p \frac{V_{\rm sec}}{V_{\text{in(min)}}} = 4 \tag{23}$$

and the magnetizing inductance and magnetizing current are calculated as

$$L_m = N_p^2 A_L = 1.6\ \text{mH} \tag{24}$$

and

$$\Delta I_m = \frac{V_{\text{in(min)}} D_{\max}}{L_m f_s} = 0.68\ \text{A}. \tag{25}$$

C. Selection of the Rectifier Diodes

From (17), the voltage stress imposed on rectifier diodes D_{r1} and D_{r2} is $V_{Dr} = V_{\rm sec}/n = 53.3$ V. When rectifier diode D_{r1} or D_{r2} is conducting, the maximum diode current

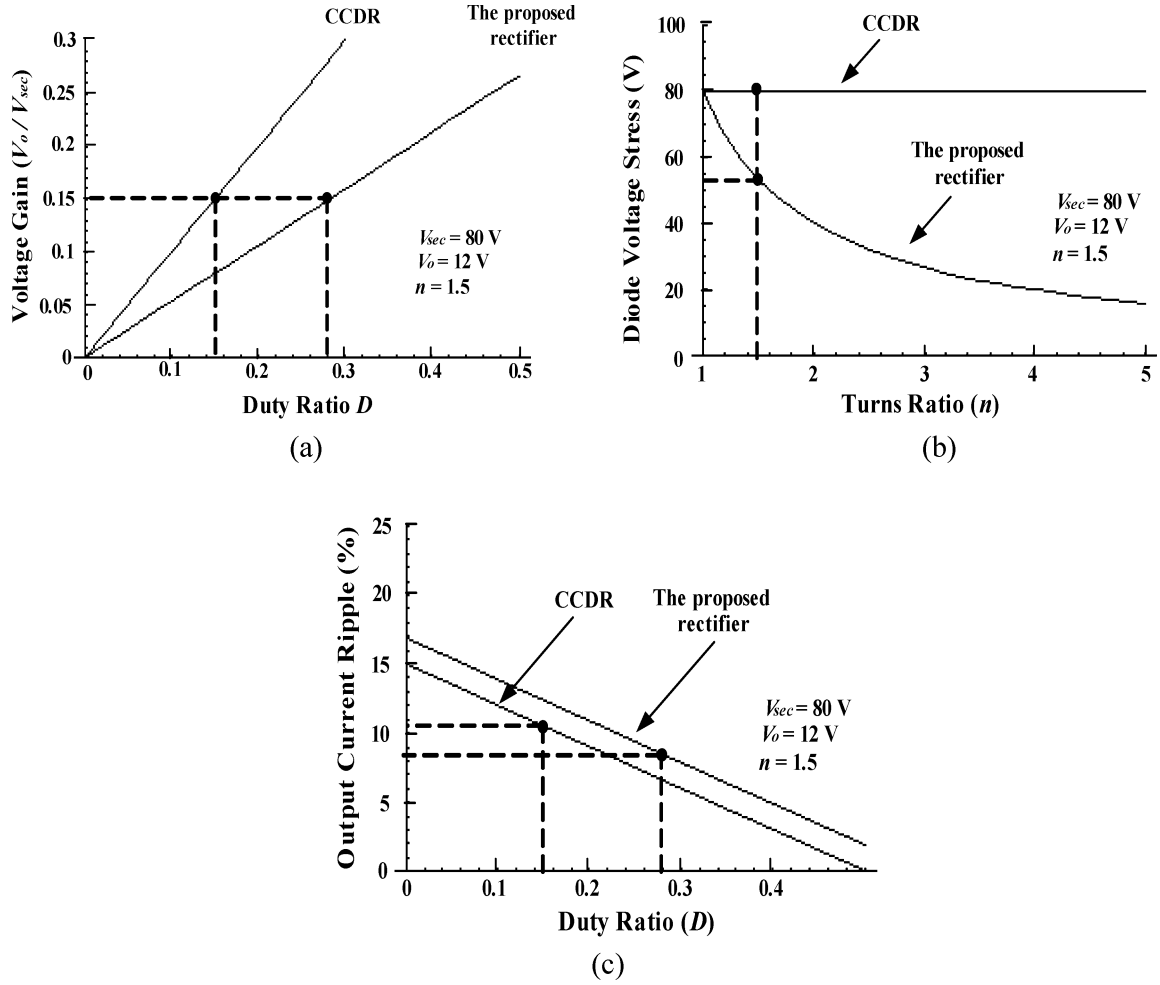

Fig. 9. Performance comparison between the proposed rectifier and the CCDR. (a) Duty ratio. (b) Diode voltage stress. (c) Output current ripple.

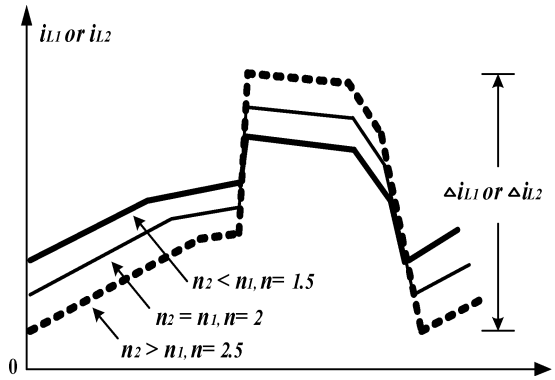

Fig. 10. Current ripple waveforms of the coupled inductor under different turns ratio n.

$i_{D(\max)} = I_{o(\max)} = 42$ A. Thus, a 63CPQ100 Schottky diode that has a low forward voltage drop ($V_F = 0.64$ V) is selected.

D. Selection of the Filter Capacitors

The capacitance is selected according to the specification of voltage ripple level ΔV_o, which is usually less than 1% of V_o. Hence, the filter capacitance can be determined as

$$C_o = \frac{I_o D_{\max} T_s}{V_o \times 1\%} = 1050\,\mu\text{F}. \tag{26}$$

E. Selection of the Power Switches

For the full-bridge phase-shift converter, the peak voltage stress imposed on power switches ($Q_1 - Q_4$) is $V_{ds(\max)} = V_{\text{in}(\max)} = 400V$. When power switches are turned on, the maximum switch current $i_{ds(\text{peak})}$ is equal to the sum of primary current $i_{\text{pri}(\text{peak})}$ and magnetizing current ΔI_m. Therefore, the $i_{ds(\text{peak})}$ can be expressed as

$$i_{ds(\text{peak})} = i_{\text{pri}(\text{peak})} + \Delta I_m = i_{\text{sec}\,(\text{peak})} \frac{N_s}{N_p} + \Delta I_m. \tag{27}$$

From Fig. 4, $i_{\text{sec}(\text{peak})}$ can be expressed as

$$\begin{aligned} i_{\text{sec}\,(\text{peak})} &= \frac{I_o}{2}\frac{n_2}{n_1} + \frac{(V_{\text{sec}(\max)} - nV_o)D_{\min}}{n^2 L f_s} \\ &= \frac{I_o}{2}\sqrt{\frac{L_{11}}{L}} + \frac{(V_{\text{sec}(\max)} - nV_o)D_{\min}}{n^2 L f_s}. \end{aligned} \tag{28}$$

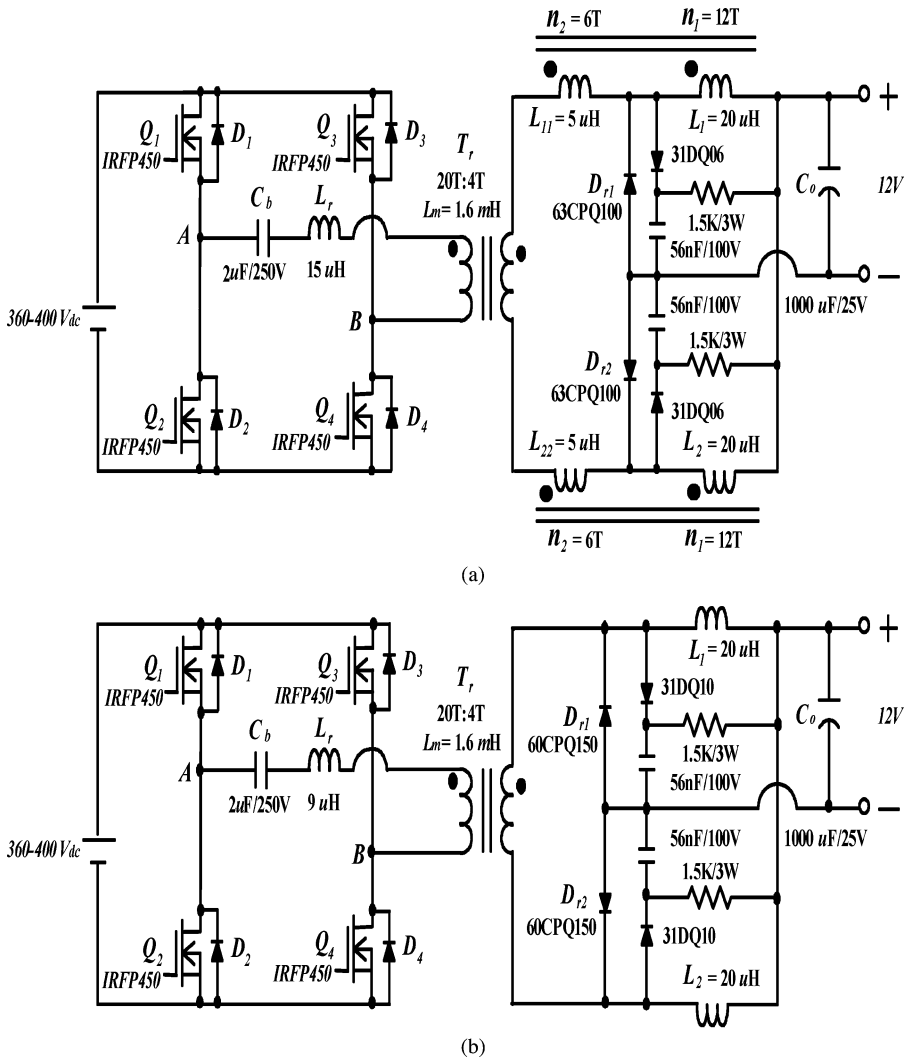

Fig. 11. Experimental circuit. (a) Proposed current-doubler rectifier with a full-bridge phase-shift converter. (b) CCDR with a full-bridge phase-shift converter.

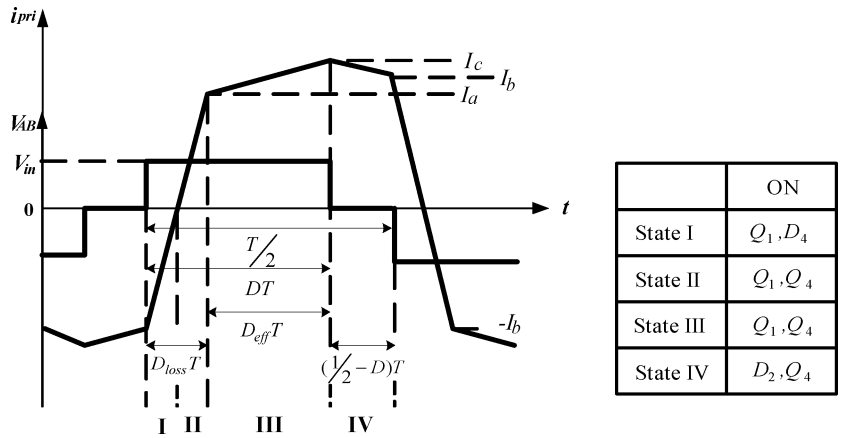

	ON
State I	Q_1, D_4
State II	Q_1, Q_4
State III	Q_1, Q_4
State IV	D_2, Q_4

Fig. 12. Primary current and voltage waveforms of the proposed rectifier with a full-bridge phase-shift converter.

By substituting the parameters into the previous equation, $i_{\mathrm{sec(peak)}}$ can be determined as 14.36 A. Thus, $i_{ds(\mathrm{peak})} = 2.87 + 0.68 = 3.55$ A. Selection of power switches involves a tradeoff between the conduction loss and switching loss. MOSFETs with low $R_{ds(\mathrm{ON})}$ can usually keep conduction loss low, but they usually have high parasitic capacitance and require a large die size. In this application, the power switches are IRFP450 with a drain–source

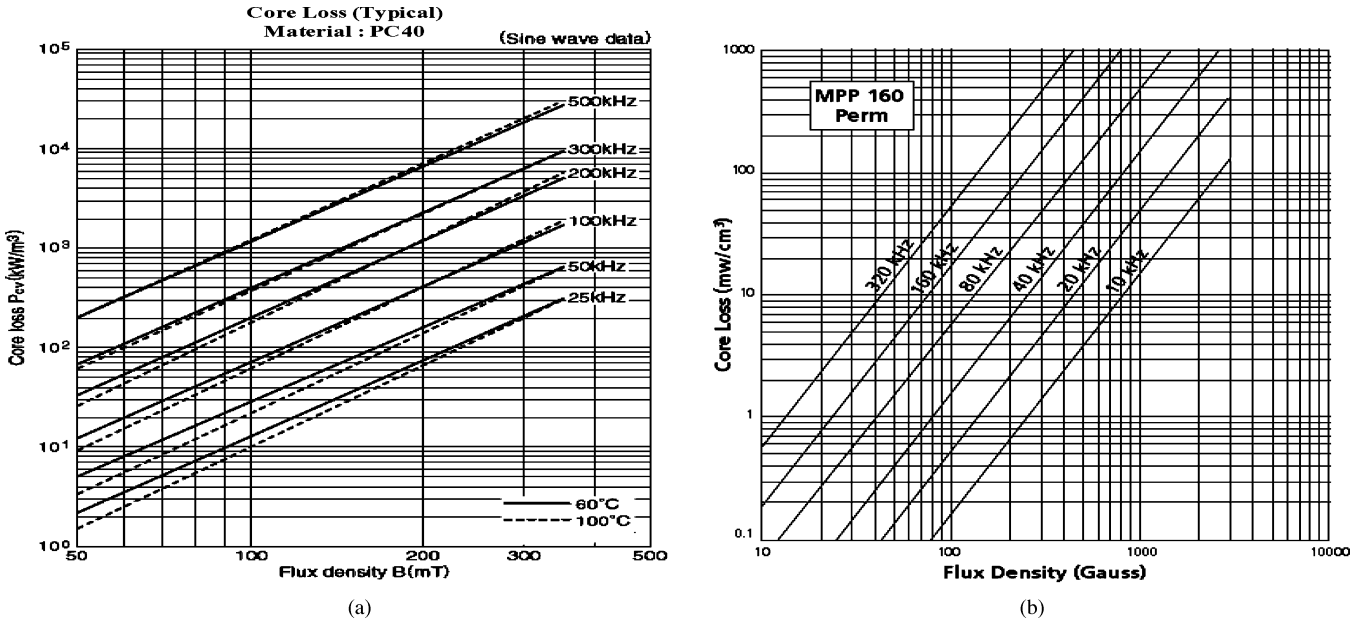

(a) (b)

Fig. 13. Typical core loss data. (a) Transformer and coupled inductor. (b) Resonant inductor.

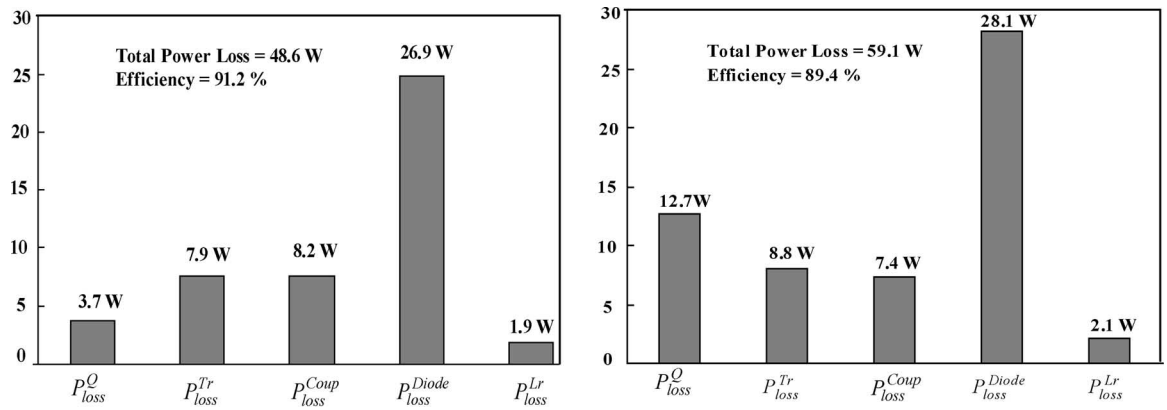

(a) (b)

Fig. 14. Estimation of power losses. (a) Proposed current-doubler rectifier with a full-bridge phase-shift converter. (b) CCDR with a full-bridge phase-shift converter.

breakdown voltage of 500 V and a channel resistance of 0.4 Ω.

F. Determination of the Resonant Capacitance and Inductance

According to [12], the parasitic capacitor ($C_{\rm oss}$) of the MOSFET switch will be multiplied by a factor $4/3$ to accommodate the increase caused by high voltage operation. During each switching transition, the output capacitance of the two switches are in parallel, and the total capacitance is equal to $8/3\ C_{\rm oss}$. From the operation, parasitic capacitance (C_{Tr}) of the isolation transformer must also be included as a part of the resonant capacitance. Therefore, the resonant capacitance of the active switch can be approximated as

$$C_r = \left[\left(\frac{8}{3}C_{\rm oss}\right) + C_{Tr}\right] = 1.4\ n{\rm F} \tag{29}$$

where the parasitic capacitance $C_{\rm oss}$ of the IRFP450 MOSFETs is about 400 pF and the isolation transformer capacitance C_{Tr} is about 0.3 nF.

In order to achieve ZVS at the turn-on transition for all of the power switches, there must be sufficient energy stored in resonant inductor L_r to completely discharge the resonant capacitors ($C_{r1} - C_{r4}$). Therefore, the following inequality must be satisfied:

$$\frac{1}{2} \times L_r \times i^2_{\rm pri(peak)} \geq \frac{1}{2} \times C_r \times V^2_{\rm in(min)}. \tag{30}$$

An approximate minimum value of the resonant inductance can be determined as

$$L_r \geq \frac{C_r \times V^2_{\rm in(min)}}{i^2_{ds(\rm peak)}} = 14.4\ \mu{\rm H} \tag{31}$$

and we select the resonant inductance $L_r = 15\ \mu$H.

V. Power Loss Estimation

In this section, power losses of the proposed rectifier with a full-bridge phase-shift converter are estimated to verify the measured efficiency. The key component values of the experimental converter are shown in Fig. 11(a), in which power losses are evaluated as follows.

A. Active Switches (Q_1–Q_4)

Power loss of the active switches includes switching loss and conduction loss. In Fig. 11(a), the active switches are turned on under ZVS and turned off under zero-voltage transition (ZVT), so that their switching loss is negligible. The conduction loss can be divided into two parts; one is channel resistance loss of the switch and the other is body diode loss of the switch. Fig. 12 shows the primary current and voltage waveforms of the full-bridge phase-shift converter, and its key equations can be expressed as

$$I_a = \frac{N_s}{N_p}\left[\frac{I_o}{2}\sqrt{\frac{L_{11}}{L}} - \frac{(V_{\sec(\max)} - nV_o)D_{\min}}{n^2 L f_s}\right] \quad (32)$$

$$I_b = \frac{N_s}{N_p}\left\{\left[\frac{I_o}{2}\sqrt{\frac{L_{11}}{L}} + \frac{(V_{\sec(\max)} - nV_o)D_{\min}}{n^2 L f_s} - \frac{V_o}{2n^2 L f_s}\left(\frac{1}{2} - D_{\min}\right)\right]\right\} \quad (33)$$

$$I_c = \frac{N_s}{N_p}\left[\frac{I_o}{2}\sqrt{\frac{L_{11}}{L}} + \frac{(V_{\sec(\max)} - nV_o)D_{\min}}{n^2 L f_s}\right] \quad (34)$$

$$D_{\text{loss}} = \frac{I_a + I_b}{(T_s/2) \times (V_{\text{in}(\max)}/L_r)} \quad (35)$$

and

$$D = D_{\text{eff}} + D_{\text{loss}} \quad (36)$$

where $D_{\text{eff}} = D_{\min}$. By substituting the parameters, as shown in Section IV, into the previous equations, they can be determined as $I_a = 1.53$ A, $I_b = 2.71$ A, $I_c = 3.55$ A, $D_{\text{loss}} = 0.026$, and $D = 0.31$. In this study, the active switches are selected as IRFP450 MOSFET, and their channel resistance $R_{ds(\text{ON})} = 0.4\ \Omega$ and body diode voltage drop $V_F = 1.4$ V. The channel resistance loss and body diode loss of the active switches can be expressed as

$$P_{Q1} = R_{ds(\text{ON})}\left[\left(\frac{I_a^2}{3} \times \frac{D_{\text{loss}}}{2}\right) + \left(\frac{I_a^2 + I_c^2 + I_a I_c}{3} \times D_{\text{eff}}\right)\right] \quad (37)$$

$$P_{Q4} = R_{ds(\text{ON})}\left[\left(\frac{I_a^2}{3} \times \frac{D_{\text{loss}}}{2}\right) + \left(\frac{I_a^2 + I_c^2 + I_a I_c}{3} \times D_{\text{eff}}\right) + \left(\frac{I_b^2 + I_c^2 + I_b I_c}{3} \times \left(\frac{1}{2} - D\right)\right)\right] \quad (38)$$

$$P_{D4} = V_F \times \left(\frac{I_b}{2} \times \frac{D_{\text{loss}}}{2}\right) \quad (39)$$

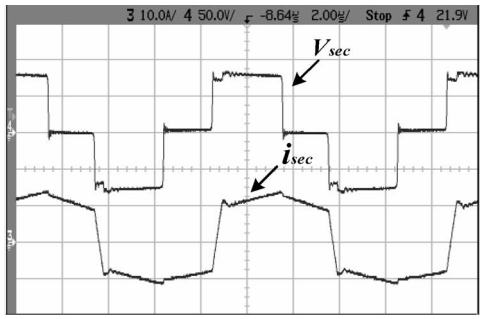

Fig. 15. Measured waveforms of the transformer secondary voltage and current ($V_{\sec}$: 50 V/div., $i_{\sec}$: 10 A/div., time: 2 μs/div.).

and

$$P_{D2} = V_F \times \left[\left(\frac{I_c - I_b}{2}\right)\left(\frac{1}{2} - D\right)\right]. \quad (40)$$

By substituting the parameters into the previous equations, the channel resistance loss and body diode loss can be determined as $P_{Q1} = 0.71$ W, $P_{Q4} = 1.01$ W, $P_{D2} = 0.12$ W, and $P_{D4} = 0.025$ W. Therefore, the total conduction loss in the four active switches can be estimated as

$$P_{\text{loss}}^{Q} = 2(P_{Q1} + P_{Q4} + P_{D2} + P_{D4}) = 2 \times 1.865 = 3.7\ \text{W}. \quad (41)$$

B. Isolation Transformer

Power loss of the isolation transformer includes core loss and copper loss. As listed in Section IV, the transformer core (PC40 ETD44) is selected with maximum flux density $B_{\max} = 200$ mT and effective core volume $V_e = 18\ \text{cm}^3$, and the switching frequency is 100 kHz. Flux density versus core loss plots of material TDK PC40 is shown in Fig. 13(a), from which we can obtain the core loss per volume, $P_{Tr(cv)} = 0.4\ \text{W/cm}^3$ at 60 °C. Thus, the core loss can be estimated as

$$P_{\text{core}}^{Tr} = P_{Tr(cv)} \times V_e = 0.4 \times 18 = 7.2\ \text{W}. \quad (42)$$

Copper loss of the isolation transformer can be expressed as

$$P_{\text{copper}}^{Tr} = (I_{ds(\text{rms})})^2 R_{\text{pri}} + (I_{\sec(\text{rms})})^2 R_{\sec} \approx \left[\begin{array}{l}\left(i_{ds(\text{peak})}\sqrt{2D_{\max}}\right)^2 R_{\text{pri}} \\ \quad + \left(i_{\sec(\text{peak})}\sqrt{2D_{\max}}\right)^2 R_{\sec}\end{array}\right]. \quad (43)$$

According to measurement, the primary winding resistance $R_{\text{pri}} = 23.8\ \text{m}\Omega$, and the secondary winding resistance $R_{\sec} = 4.2\ \text{m}\Omega$ at 100 kHz. Thus, the copper loss is 0.7 W. The total power loss of the isolation transformer can be determined as

$$P_{\text{loss}}^{Tr} = P_{\text{core}}^{Tr} + P_{\text{copper}}^{Tr} = 7.2 + 0.7 = 7.9\ \text{W}. \quad (44)$$

C. Coupled Inductors

Cores of the coupled inductors are TDK PC40 ETD39 ($A_e = 1.25\ \text{cm}^2$, $A_w = 2.57$ cm, and $V_e = 11.5\ \text{cm}^3$). Their primary winding turns are $n_p = (n_1 + n_2) = 18$, secondary winding

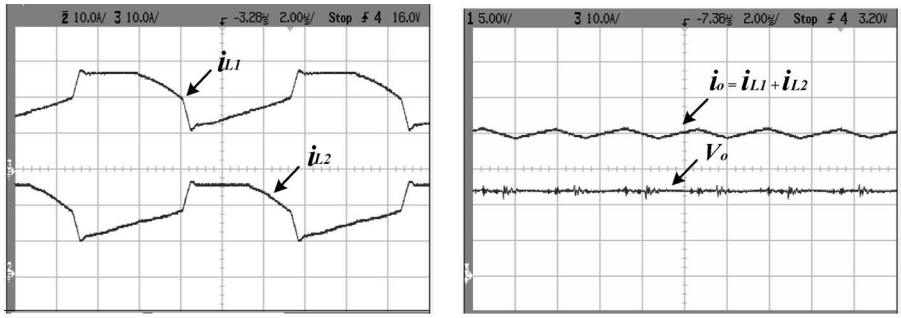

(a) (b)

Fig. 16. Measured waveforms. (a) Inductor currents i_{L1} and i_{L2}, (i_{L1} : 10 A/div., i_{L2} : 10 A/div., time: 2 μs/div.). (b) Output current i_o ($= i_{L1} + i_{L2}$) and output voltage (i_o : 10 A/div., V_o : 5 V/div., time: 2 μs/div.).

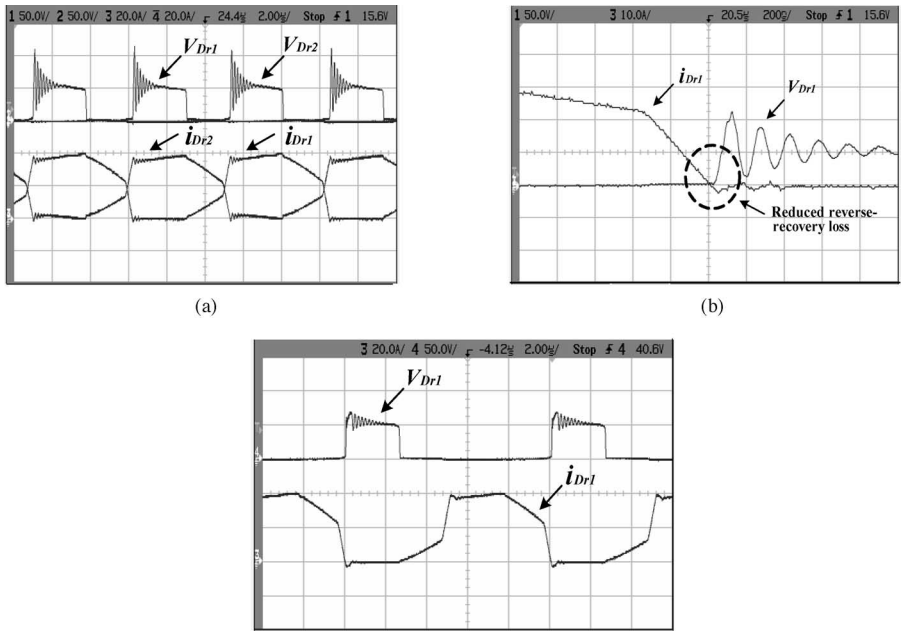

(a) (b) (b)

Fig. 17. Measured waveforms of the voltage and current of the rectifier diodes. (a) Without RCD snubber (V_{Dr} : 50 V/div., i_{Dr} : 20 A/div., time: 2 μs/div.). (b) Its extended waveforms (V_{Dr1} : 50 V/div., i_{Dr1} : 10 A/div., time: 200 ns/div.). (c) With RCD snubber (V_{Dr1} : 50 V/div., i_{Dr1} : 20 A/div., time: 2 μs/div.).

turns are $n_s = n_1 = 6$, and turns ratio $n = n_p/n_s = 1.5$. Thus, the maximum flux density can be determined as

$$B_{\max}^{\text{Coup}} = \frac{n^2 L \times \Delta i_L}{n_p \times A_e} = \frac{1.5^2 \times 20 \times 10^{-6} \times 3.86}{18 \times 1.25} \times 10^8 = 772 \text{ G} \quad (45)$$

where

$$\Delta i_L = \frac{(V_{\text{sec(max)}} - nV_o)D_{\min}}{n^2 L f_s} = 3.9 \text{ A}. \quad (46)$$

Again from Fig. 13(a), we can obtain the core loss per volume $P_{\text{Coup(cv)}} = 0.04 \text{ W/cm}^3$ at 60 °C. The core loss will be

$$P_{\text{core}}^{\text{Coup}} = P_{\text{Coup}(cv)} \times V_e = 0.04 \times 11.5 = 0.5 \text{ W}. \quad (47)$$

According to measurement, winding resistance of the coupled inductors $R_{\text{Coup}} = 8.2 \text{ m}\Omega$, and the copper loss can be estimated as

$$P_{\text{copper}}^{\text{Coup}} = \left(\frac{I_o}{2}\right)^2 R_{\text{Coup}} = \left(\frac{42}{2}\right)^2 \times 8.2 \times 10^{-3} = 3.6 \text{ W}. \quad (48)$$

Therefore, the total power loss of the coupled inductors is

$$P_{\text{loss}}^{\text{Coup}} = 2(P_{\text{core}}^{\text{Coup}} + P_{\text{copper}}^{\text{Coup}}) = 2(0.46 + 3.62) = 8.2 \text{ W}. \quad (49)$$

D. Rectifier Diodes

The rectifier diodes are selected as 63CPQ100 Schottky diodes with forward voltage drop $V_F = 0.64$ V. Thus, the total

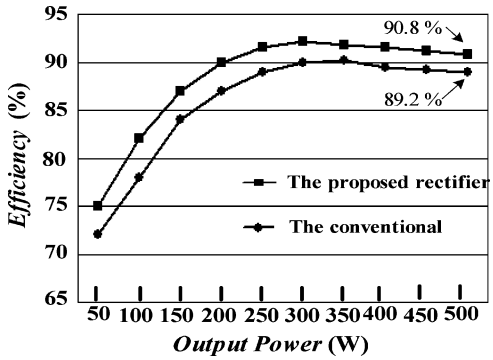

Fig. 18. Efficiency comparison between the proposed and the conventional current doublers associated with a full-bridge converter.

conduction loss of the rectifier diodes is

$$P_{\text{loss}}^{\text{Diode}} = I_o \times V_F = 42 \times 0.64 = 26.9 \text{ W}. \quad (50)$$

E. Resonant Inductor

The core of the resonant inductor is selected as ARNOLD A-643136-2 ($A_e = 0.552\,\text{cm}^2$, $l_e = 8.147\,\text{cm}$, and $V_e = 4.49\,\text{cm}^3$), and its winding turns $N_{Lr} = 8$. By applying the Faraday's law, the actual maximum flux density can be determined as

$$B_{Lr(\max)} = \frac{V_{\text{in}(\max)} \times D_{\text{loss}} T_s}{2N_{Lr} \times A_e} \times 10^8 = 815 \text{ G}. \quad (51)$$

By referring to flux density versus core loss plots of core A-643136-2 as shown in Fig. 13(b), we can obtain the core loss per volume $P_{Lr(cv)} = 0.4\,\text{W/cm}^3$. Thus, the core loss can be estimated as

$$P_{\text{core}}^{Lr} = P_{Lr(cv)} \times V_e = 0.4 \times 4.49 = 1.8 \text{ W}. \quad (52)$$

According to measurement, the winding resistance $R_{Lr} = 25.7\,\text{m}\Omega$, and the copper loss of the resonant inductor will be

$$P_{\text{copper}}^{Lr} = I_{ds(\text{rms})}^2 \times R_{Lr} = 0.1 \text{ W}. \quad (53)$$

The total power loss of the resonant inductor will then be

$$P_{\text{loss}}^{Lr} = P_{\text{core}}^{Lr} + P_{\text{copper}}^{Lr} = 1.8 + 0.1 = 1.9 \text{ W}. \quad (54)$$

Finally, the estimated total power loss and efficiency of the proposed current-doubler rectifier with a full-bridge phase-shift converter are determined as

$$P_{\text{loss}}^{\text{Total}} = P_{\text{loss}}^{Q} + P_{\text{loss}}^{Tr} + P_{\text{loss}}^{\text{Coup}} + P_{\text{loss}}^{\text{Diode}} + P_{\text{loss}}^{Lr} = 48.6 \text{ W} \quad (55)$$

and

$$\eta^{\text{Total}} = \frac{P_o}{P_{\text{loss}}^{\text{Total}} + P_o} = 91.2\%. \quad (56)$$

Breakdown of the total power losses of the CCDR [5] and that of the proposed rectifier under full-load condition are illustrated in Fig. 14, from which it can be seen that the proposed rectifier can reduce switch loss significantly and improve the overall power conversion efficiency.

VI. Experimental Results

The proposed rectifier with a full-bridge phase-shift converter has been verified on a 500-W prototype. The component values of the experimental converter are shown in Fig. 11(a), and a UC3875 controller is used to implement the phase-shift control circuit. To highlight the merits of the proposed rectifier, a CCDR shown in Fig. 11(b) was also implemented.

Fig. 15 shows measured voltage and current waveforms at the secondary side of the transformer. Fig. 16(a) shows measured current waveforms of inductors L_1 and L_2, and Fig. 16(b) shows output voltage and full-load output current with low ripple. Fig. 17(a) shows measured voltage and current waveforms of the rectifier diodes, from which a severe voltage overshoot and ringing are observed due to the oscillation between leakage inductance of the coupled inductors and junction capacitance of the rectifier diodes. The voltage overshoot and ringing can be damped by a simple resistor–capacitor–diode (RCD) snubber circuit, as shown in Fig. 11(a). Fig. 17(b) shows its extended waveforms and illustrates a small reverse recovery loss. Fig. 17(c) shows those with RCD snubbers, where the spike voltage of the rectifier has been clamped. Fig. 18 shows efficiency measurements of the proposed rectifier as compared with a conventional one, from which it can be seen that the maximum efficiency of the proposed rectifier can reach as high as 90.8% under full-load condition. Notice that the measured efficiency from the proposed rectifier is very close to the estimated value of 91.2%. The proposed rectifier is relatively feasible for converters with high step-down voltage ratio and requiring high power density, which has been verified by the experimental results.

VII. Conclusion

In this paper, an improved current-doubler rectifier with coupled inductors has been proposed and analyzed. In comparison with the CCDR, the proposed rectifier has the merits of low output current ripple and extended duty ratio, which can reduce the peak current through the isolation transformer and switches, the conduction loss in the switches, and the copper loss in the isolation transformer. Furthermore, the low voltage stress of the rectifier diode can reduce reverse recovery loss. Experimental results have verified that the proposed rectifier can achieve high efficiency over a wide load range. It is relatively suitable for high step-down voltage ratio and high output current applications.

References

[1] Intel Corporation, The micro-architecture of the Pentium 4 processor, in Proc. Intel Technology Symposium. (2001). [Online]. Available: http://download.intel.com/technology/itj/q12001

[2] H. K. Ji and H. J. Kim, "Active clamp forward converter with MOSFET synchronous rectification," in *Proc. Power Electron. Spec. Conf.*, Jun. 1994, pp. 895–901.

[3] V. Tuomainen and J. Kyyrä, "Effect of resonant transition on efficiency of forward converter with active clamp and self-driven SRs," *IEEE Trans. Power Electron.*, vol. 20, no. 2, pp. 315–323, Mar. 2005.

[4] Q. M. Li and F. C. Lee, "Design consider of the active-clamp forward converter with current mode control during large-signal transient," *IEEE Trans. Power Electron.*, vol. 18, no. 4, pp. 958–965, Jul. 2003.

[5] N. H. Kutkut, D. M. Divan, and R. W. Gascoigne, "An improved full bridge zero voltage switching PWM converter using a two-inductor rectifier," *IEEE Trans. Ind. Appl.*, vol. 31, no. 1, pp. 119–126, Jan./Feb. 1995.

[6] Y. Jang, M. M. Jovanović, and Y. M. Chang, "A new ZVS-PWM full-bridge converter," *IEEE Trans. Power Electron.*, vol. 18, no. 5, pp. 1122–1129, Sep. 2003.
[7] J. A. Sabate, V. Vlatkovic, R. B. Ridley, F. C. Lee, and B. H. Cho, "Design considerations for high-voltage high-power full-bridge zero-voltage-switching PWM converter," in *Proc. Appl. Power Electron. Conf.*, Mar. 1990, pp. 275–284.
[8] R. Redl, N. O. Sokal, and L. Balogh, "A novel soft-switching full-bridge DC/DC converter: Analysis, design considerations, and experimental results at 1.5 kW, 100 kHz," *IEEE Trans. Power Electron.*, vol. 6, no. 3, pp. 408–418, Jul. 1991.
[9] G. Hua, F. C. Lee, and M. M. Jovanović, "An improved full-bridge zero-voltage-switched PWM converter using a saturable inductor," *IEEE Trans. Power Electron.*, vol. 8, no. 4, pp. 530–534, Oct. 1993.
[10] R. Redl, L. Balogh, and D. W. Edwards, "Optimum ZVS full-bridge DC/DC converter with PWM phase-shift control: Analysis, design considerations, and experimental results," in *Proc. Appl. Power Electron. Conf.*, Feb. 1994, pp. 159–165.
[11] E.-S. Kim, K.-Y. Joe, M.-H. Kye, Y.-H. Kim, and B.-D. Yoon, "An improved soft-switching PWM FB DC/DC converter for reducing conduction losses," *IEEE Trans. Power Electron.*, vol. 14, no. 2, pp. 258–263, Mar. 1999.
[12] B. Andreycak, "Phase shifted, zero voltage transition design considerations and the UC3875 PWM controller," Unitrode Application Note U-136A, Unitrode, CA, 1997.

Tsai-Fu Wu (S'88–M'91–SM'98) received the B.S. degree in electronic engineering from the National Chiao-Tung University, Hsinchu, Taiwan, in 1983, the M.S. degree in electrical and computer engineering from Ohio University, Athens, in 1988, and the Ph.D. degree in electrical engineering and computer science from the University of Illinois, Chicago, in 1992.

From 1985 to 1986, he was a System Engineer at SAMPO, Inc., Taiwan, where he was engaged in developing and designing graphic terminals. From 1988 to 1992, he was a Teacher and a Research Assistant in the Department of Electrical Engineering and Computer Science (EECS), University of Illinois, Chicago. Since 1993, he has been with the Department of Electrical Engineering, National Chung Cheng University, Chia-Yi, Taiwan, where he is currently a Professor and the Director of the Elegant Power Application Research Center (EPARC). His current research interests include developing and modeling of power converters, design of electronic dimming ballasts for fluorescent lamps, metal halide lamps and plasma display panels, design of solar-array supplied inverters for grid connection, and design of pulsed-electrical-field generators for transdermal drug delivery and food pasteurization.

Prof. Wu received three Best Paper Awards from Taipei Power Electronics Association in 2003–2005. In 2005, he was rated as one of the top 5% outstanding researchers by the National Science Council, Taiwan. He is a Senior Member of the International Commission on Illumination (CIE).

Cheng-Tao Tsai received the B.S. degree in electrical engineering in 1991 from Feng Chia University, Taichung, Taiwan and the M.S. degree in electrical engineering in 2003 from the National Chung Cheng University, Chia-Yi, Taiwan, where he is currently working toward the Ph.D. degree in the Department of Electrical Engineering.

His current research interests include design of switching-mode power supplies, power factor correction technology, and chargers for electric vehicles.

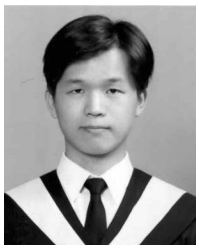

Yong-Dong Chang received the B.S. and M.S. degrees in electrical engineering in 2002 and 2004, respectively, from Kun Shan University, Tainan, Taiwan. He is currently working toward the Ph.D. degree in the Department of Electrical Engineering at National Chung Cheng University, Chia-Yi, Taiwan.

His current research interests include design and implementation of resonant converters for battery chargers, and pulsed voltage generator application for liquid food sterilization.

Yaow-Ming Chen (S'96–M'98–SM'05) received the B.S. degree from the National Cheng-Kung University, Tainan, Taiwan, in 1989, and the M.S. and Ph.D. degrees from the University of Missouri, Columbia, in 1993 and 1997, respectively, all in electrical engineering.

From 1997 to 2000, he was with I-Shou University, Taiwan, as an Assistant Professor. In 2000, he joined the National Chung Cheng University, Chia-Yi, Taiwan, where he is currently an Associate Professor in the Department of Electrical Engineering. His current research interests include power electronic converters, power system harmonics and compensation, and intelligent control.

Dr. Chen is a Senior Member of the IEEE Power Electronics and the IEEE Industrial Electronics Societies.